PERGAMON

International Journal of Multiphase Flow 27 (2001) 2129–2153

International Journal of Multiphase Flow

www.elsevier.com/locate/ijmulflow

Two-way coupling of Eulerian–Lagrangian model for dispersed multiphase flows using filtering functions

Atsuhide Kitagawa *, Yuichi Murai, Fujio Yamamoto

Department of Mechanical Engineering, Fukui University, Bunkyo 3-9-1, Fukui 910-8507, Japan

Received 1 December 2000; received in revised form 27 May 2001

Abstract

Eulerian–Lagrangian approaches for dispersed multiphase flows can simulate detailed flow structures with a much higher spatial resolution than the Eulerian–Eulerian approaches. However, there are still unsolved problems regarding the calculation method for accurate two-way interaction, especially on the numerical instability due to the dispersion migration through discrete computational grids. Inadequate solvers sometimes produce false velocity fluctuation which makes the simulation unstable. In this paper, a new calculation method for dispersion-to-continuous phase interaction, which is accompanied by spherical dispersion migration, is proposed. The basic principle of the method is the introduction of Lagrangian filtering functions which convert discrete dispersion volume fractions to a spatially differentiable distribution. The performance of linear, Gaussian and sinewave filtering functions is examined by simple benchmark tests and applied to the simulation of dispersion-generated fluctuation. Using the present method, three-dimensional continuous phase flow structures induced by rising spherical bubbles and/or settling solid particles are demonstrated.

Keywords: Numerical analysis; Dispersed multiphase flow; Dispersion-generated velocity fluctuation; Natural convection; Turbulent flow; Computational fluid dynamics; Finite differential method; Eulerian–Lagrangian model

1. Introduction

Numerical methods for dispersed multiphase flows have played an important role for analyzing alternation mechanisms of various flow regimes due to the inclusion of dispersions, such as bubbles, drops, and particles. Nowadays, a number of numerical methods for dispersed multiphase flows have been proposed as follows. Direct numerical simulations (DNSs) of

* Corresponding author. Tel.: +81-776-23-0500x 2687.
E-mail address: kitagawa@fv.mech.fukui-u.ac.jp (A. Kitagawa).

0301-9322/01/$ - see front matter
PII: S0301-9322(01)00040-4

multiphase flows, for which the basic equations are constructed with no turbulent flow model and no interface model, are quite powerful tools to elucidate microscopic interaction mechanisms. For instance, turbulent structures accompanied by very fine particles whose sizes are much smaller than the smallest length scale of the continuous phase can be analyzed, e.g., Squires and Eaton (1990) and Elghobashi and Truesdell (1993). The DNS for a channel flow with large particles was demonstrated by Pan and Banerjee (1997) based on Stokesian dynamics. For bubbly two-phase flow, Unverdi and Tryggvason (1992) directly solved deformable bubbles using a front-tracking method. The motions of several bubbles were numerically analyzed using the level-set method (Sussman et al., 1994), the interface tracking method (Tomiyama et al., 1999), the volume of fluid (VOF) method (Tomiyama et al., 1993), and other interface-handling schemes (e.g., Kunugi, 1997). However, because of the following two reasons the DNS for bubbly flows usually produces a large computational load and needs an appropriate technique in contrast to particulate multiphase flow. One is the very short relaxation time of the bubble motions in liquids compared to that of solid particles or liquid drops. Another is the deformability of the bubble interface. The large density ratio of the gas bubble to the surrounding liquid also makes the DNS difficult. Eulerian–Eulerian types of governing equations such as the two-fluid model (e.g., Druzhinin and Elghobashi, 1998) and the drift-flux model (e.g., Ransom, 1985) have been employed over a long time in nuclear-related research. These models obtain grid-averaged flow structures of gas–liquid two-phase flows, and derive valid transient flow characteristics when adequate constitution equations are employed. However, detailed mechanisms of instantaneous and local phase interaction processes are not explored by Eulerian–Eulerian models. Ensemble-averaged equations which are explained by Zhang and Prosperetti (1994) are known as a exact mathematical expression of dispersed multiphase flow in the Eulerian–Eulerian form.

Over the last decade Eulerian–Lagrangian models (E–L models, in abbreviation) have already been applied to many kinds of dispersed multiphase flows (e.g., Reutsch and Meiburg, 1994; Valentine and Decker, 1995, etc.). Since the E–L model employs the Lagrangian tracking method for calculating each dispersion trajectory, it can simulate phase interaction with a much higher spatial resolution than Eulerian–Eulerian model. The E–L models which are currently published in the literature can be classified in three kinds. First is the DNS-type E–L model, second is the Reynolds-averaged-type E–L model, and third is the large eddy simulation (LES)-type E–L model. The DNS-type E–L model is constructed with the ordinary conservation law for each phase without any turbulent flow model. Nadaoka et al. (1999) and Murai et al. (2000a,b) succeeded in simulating buoyancy-generated velocity fluctuation in bubbly flow based on the DNS-type E–L model. Reynolds-averaged E–L models using k–ε transportation equations were proposed by Moissette et al. (2000) and Decker and Sommerfeld (2000). LES-type E–L models were proposed by Sugiyama and Matsumoto (1998) and Nadaoka et al. (1999). However, the generality of their turbulent flow models is still in discussion.

Currently, however, the E–L model has the following problems in terms of dispersion-to-continuous phase interaction. (1) When a dispersion passes through the interface of the computational grid, false fluctuations of the continuous phase velocity is caused by sudden changes of the local volume fraction. In the case of large dispersions, the computation often collapses due to the numerical instability. (2) When a small grid is applied in order to improve the spatial resolution, the amplitude of the false velocity fluctuation becomes large. In fact, the

applicability of the E–L model is restricted by this problem especially for boundary layer issues which need fine grid systems in the vicinity of the boundary, and for complicated flow geometries which need generalized curvilinear coordinate systems using fine meshes. The fundamental reason of the aforementioned two problems are related to the mathematically inappropriate procedure of the E–L model in which both Eulerian-type and Lagrangian-type equations are combined and solved as simultaneous differential equations.

In this paper, three kinds of techniques for removing the false velocity fluctuation and improving the numerical accuracy are proposed. The basic principle of the present method is to transform the local volume fraction which is obtained independently at each grid, into a spatially differentiable distribution. Linear, Gaussian, and sinewave functions have been considered as the filtering function. The performance of these functions are theoretically examined by single dispersion migration. Finally, the present DNS-type E–L model based on the Lagrangian filtering function is applied to the three-dimensional simulation of dispersion-generated velocity fluctuation. The demonstrated results show good analogy with experimental observations, and revealed several qualitative features of the dispersion-generated velocity fluctuation.

2. Governing equations of the Eulerian–Lagrangian model

The objective flow treated in this paper is a three-dimensional unsteady flow which involves bubbles and/or particles in an incompressible viscous liquid. The translational motion of the dispersion is tracked by using a Lagrangian-type equation, while the conservation laws of physical quantities in the liquid phase are expressed by Eulerian-type equations.

2.1. Assumptions

All the equations are constructed under the following assumptions:

1. Bubbles and particles are spherical. Reynolds number of the dispersion is lower than 100.
2. Coalescence and fragmentation of bubbles do not happen. The maximum void fraction is lower than 0.03.
3. Interactive forces between dispersions are ignored. That is, bubble–bubble, particle–particle, and bubble–particle interactions are neglected.
4. There is no mass transfer through the surface of particles and bubbles.
5. The flow field is isothermal.

2.2. Governing equations

Conservation equation for the liquid mass:

$$\frac{\partial \alpha_L \rho_L}{\partial t} + \nabla \cdot \alpha_L \rho_L \mathbf{u}_L = 0, \tag{1}$$

where α_L is the liquid volume fraction and $\mathbf{u}_L$ is the liquid velocity vector. The liquid density ρ_L is constant. These variables are grid-averaged in Eulerian frame.

Gas volume fraction is defined as

$$\alpha_G = \frac{1}{V}\int_V \alpha_{G,Local}\, dV, \tag{2}$$

where $\alpha_{G,Local}$ is a phase indicator, i.e., it takes the value of 1 for the gas phase and 0 for the non-gas phase. V is the volume of grid.

Solid volume fraction is similarly defined as

$$\alpha_S = \frac{1}{V}\int_V \alpha_{S,Local}\, dV, \tag{3}$$

where $\alpha_{S,Local}$ is a phase indicator, i.e., it takes the value of 1 for the solid phase and 0 for the non-solid phase. Detailed calculation methods for Eqs. (2) and (3) are explained in Section 3.

Equation for tracking each bubble position is

$$\mathbf{x}_G = \mathbf{x}_G(0) + \int_0^t \mathbf{u}_G\, dt. \tag{4}$$

Equation for tracking each particle position is

$$\mathbf{x}_S = \mathbf{x}_S(0) + \int_0^t \mathbf{u}_S\, dt. \tag{5}$$

Here $\mathbf{u}_G$ in Eq. (4) is velocity of individual bubble, and $\mathbf{u}_S$ in Eq. (5) is that of individual particle. These velocity vectors are defined at the center of gravity of each dispersion.

Conservation equation of the total momentum:

$$\begin{aligned}&\frac{\partial \alpha_L \rho_L \mathbf{u}_L}{\partial t} + \nabla\cdot\alpha_L\rho_L\mathbf{u}_L\mathbf{u}_L + \frac{\partial \alpha_G \rho_G \mathbf{u}_G}{\partial t} + \nabla\cdot\alpha_G\rho_G\mathbf{u}_G\mathbf{u}_G + \frac{\partial \alpha_S \rho_S \mathbf{u}_S}{\partial t} + \nabla\cdot\alpha_S\rho_S\mathbf{u}_S\mathbf{u}_S \\ &\quad = -\nabla p - (\alpha_L\rho_L + \alpha_G\rho_G + \alpha_S\rho_S)\mathbf{g} + (\mathbf{F}_{LL} + \mathbf{F}_{GG} + \mathbf{F}_{SS}),\end{aligned} \tag{6}$$

where $\mathbf{u}_G$ and $\mathbf{u}_S$ are the gas and the solid phase velocities defined by grid-averaged value which is calculated by averaging of the velocities of dispersions in each grid; ρ_G and ρ_S are the densities of the gas and the solid phases; p is the pressure and $\mathbf{g}$ is the gravitational acceleration; $\mathbf{F}_{LL}$, $\mathbf{F}_{GG}$, and $\mathbf{F}_{SS}$ are shear stress forces in the liquid, gas, and solid phases, respectively. Here the former is given by

$$\mathbf{F}_{LL} = \nabla\cdot\mu\left(\nabla\mathbf{u}_L + \nabla\mathbf{u}_L^T - \frac{2}{3}(\nabla\cdot\mathbf{u}_L)\mathbf{I}\right). \tag{7}$$

$\mathbf{F}_{GG}$ and $\mathbf{F}_{SS}$ are 0 because interactions among dispersions are ignored. μ is the effective three-phase flow viscosity which is expressed by the following equation:

$$\mu = \left(1 + \alpha_G + \frac{5}{2}\alpha_S\right)\mu_L. \tag{8}$$

This description is theoretically derived for small dispersion Reynolds number as Batchelor (1967) explained.

The equation of bubble translational motion is

$$\frac{\mathrm{d}}{\mathrm{d}t}(\rho_{\mathrm{G}k}V_{\mathrm{G}k}\mathbf{u}_{\mathrm{G}k}) + \frac{\mathrm{d}}{\mathrm{d}t}(\beta\rho_{\mathrm{L}}V_{\mathrm{G}k}\mathbf{u}_{\mathrm{G}k}) - \frac{\mathrm{D}_{\mathrm{L}}}{\mathrm{D}t}(\beta\rho_{\mathrm{L}}V_{\mathrm{G}k}\mathbf{u}_{\mathrm{L}}) + \rho_{\mathrm{G}k}V_{\mathrm{G}k}\mathbf{g} + V_{\mathrm{G}k}\nabla p$$
$$- V_{\mathrm{G}k}\mu\left(\nabla^2\mathbf{u}_{\mathrm{L}} + \frac{1}{3}\nabla(\nabla\cdot\mathbf{u}_{\mathrm{L}})\right) + \frac{1}{2}\rho_{\mathrm{L}}(\pi r_{\mathrm{G}k}^2)C_{\mathrm{DG}}|\mathbf{u}_{\mathrm{G}k} - \mathbf{u}_{\mathrm{L}}|(\mathbf{u}_{\mathrm{G}k} - \mathbf{u}_{\mathrm{L}})$$
$$+ \frac{1}{2}\rho_{\mathrm{L}}V_{\mathrm{G}k}(\mathbf{u}_{\mathrm{G}k} - \mathbf{u}_{\mathrm{L}}) \times (\nabla \times \mathbf{u}_{\mathrm{L}}) = \mathbf{0}. \tag{9}$$

The equation of particle translational motion is

$$\frac{\mathrm{d}}{\mathrm{d}t}(\rho_{\mathrm{S}k}V_{\mathrm{S}k}\mathbf{u}_{\mathrm{S}k}) + \frac{\mathrm{d}}{\mathrm{d}t}(\beta\rho_{\mathrm{L}}V_{\mathrm{S}k}\mathbf{u}_{\mathrm{S}k}) - \frac{\mathrm{D}_{\mathrm{L}}}{\mathrm{D}t}(\beta\rho_{\mathrm{L}}V_{\mathrm{S}k}\mathbf{u}_{\mathrm{L}}) + \rho_{\mathrm{S}k}V_{\mathrm{S}k}\mathbf{g} + V_{\mathrm{S}k}\nabla p$$
$$- V_{\mathrm{S}k}\mu\left(\nabla^2\mathbf{u}_{\mathrm{L}} + \frac{1}{3}\nabla(\nabla\cdot\mathbf{u}_{\mathrm{L}})\right) + \frac{1}{2}\rho_{\mathrm{L}}(\pi r_{\mathrm{S}k}^2)C_{\mathrm{DS}}|\mathbf{u}_{\mathrm{S}k} - \mathbf{u}_{\mathrm{L}}|(\mathbf{u}_{\mathrm{S}k} - \mathbf{u}_{\mathrm{L}})$$
$$+ 3.23\mu_{\mathrm{L}}r_{\mathrm{S}k}\sqrt{Re_{\mathrm{S}}}(\mathbf{u}_{\mathrm{S}k} - \mathbf{u}_{\mathrm{L}}) \times \frac{\boldsymbol{\omega}}{|\boldsymbol{\omega}|} = \mathbf{0}, \tag{10}$$

where k indicates a label number of each dispersion,

$$\beta = \frac{1}{2}, \tag{11}$$

$$Re_{\mathrm{S}} = \frac{(2r_{\mathrm{S}})^2|\boldsymbol{\omega}|}{\nu_{\mathrm{L}}}, \tag{12}$$

$$\boldsymbol{\omega} = \nabla \times \mathbf{u}_{\mathrm{L}}, \tag{13}$$

$$C_{\mathrm{DG}} = \frac{16}{Re}\left(1 + 0.122\,Re^{0.55}\right), \tag{14}$$

$$C_{\mathrm{DS}} = \frac{24}{Re} + \frac{4.0}{\sqrt{Re}} + 0.4, \tag{15}$$

where β is an added mass coefficient for a sphere, which is theoretically given by a linearized version of the Euler equation. For the drag coefficient of bubbles, Eq. (14) proposed by Takemura and Yabe (1997) is employed. This equation is obtained by experiments with clean bubbles and applicable for a wide range of the Reynolds number from nearly 0 to 200. The drag coefficient of solid particles are given by Eq. (15), which is an experimental formula of Brauer and Mewes (1972). Auton's lift force (Auton, 1987) and Saffman's lift force (Saffman, 1965) are adopted for lift forces on bubbles and particles, respectively. The history force on bubbles is neglected since it does not work in the case of low Reynolds numbers under 50 (Takagi and Matsumoto, 1996). The Basset force on particle is also tentatively ignored in this paper owing to the heavy computational load for integrating the kernel. Although the exactness of the constitution equations should be further improved, we believe the current models are sufficient for consideration of two-way coupling method.

We use the restricting condition on the volume fraction for three-phase flow to close the equation system as

$$\alpha_L + \alpha_G + \alpha_S = 1. \tag{16}$$

2.3. Numerical procedures

The highly simplified marker and cell (HSMAC) method is extended for this set of equations. The three-dimensional cubic interpolated propagation (CIP) scheme proposed by Takewaki and Yabe (1987) is applied for all the advection terms in the equations of liquid phase. The CIP scheme calculates the discontinuous distribution accurately with high spatial resolution. For the time-integration of the translational velocity of each dispersion, a second order Crank–Nicolson scheme is employed. The detailed calculation procedures are as follows:

1. The translational velocity vector of each dispersion is calculated by Eqs. (9) and (10) with Eqs. (11)–(15).
2. The position of the center of gravity for each dispersion is calculated by Eqs. (4) and (5).
3. The distribution of the dispersion volume fraction is obtained by Eqs. (2) and (3).
4. The liquid velocity vector is calculated by Eq. (6).
5. The liquid volume fraction is obtained from Eq. (1).
6. The volume fraction error $\varepsilon = \alpha_L + \alpha_G + \alpha_S - 1$ is calculated from Eq. (16).
7. The pressure correction value $[p']$ is calculated by the following equation in accordance with the HSMAC method. Here Δx, Δy, Δz, and Δt stand for the grid intervals in three-dimensional coordinates and the differentiation time interval, respectively:

$$p' = \frac{\varepsilon}{2\Delta t^2\left(\frac{1}{\Delta x^2} + \frac{1}{\Delta y^2} + \frac{1}{\Delta z^2}\right)}. \tag{17}$$

8. After the liquid velocity is corrected by the following equation, the calculation returns to step (5) of the procedure. Here $\mathbf{u}_L^*$ is a predicted value before the correction. The iteration of this correction is performed until ε becomes smaller than the allowable error. When ε converges, the calculation for getting the next time step solution is performed by going back to step (1) of the procedure.

$$\alpha_L \mathbf{u}_L = \alpha_L \mathbf{u}_L^* - \Delta t \nabla p'. \tag{18}$$

3. Higher order two-way coupling for the Eulerian–Lagrangian model

In this section, dispersion-generated velocity fluctuation is classified into several fluid dynamic processes and new calculation methods for the two-way coupling of the E–L model are proposed.

3.1. Phenomenological classification of dispersion-generated velocity fluctuation

The velocity fluctuation of the continuous phase induced by dispersions is essentially different from that of turbulent flows. This is observed as a combined effect of several factors. In the case of bubbles, the bubble-induced velocity fluctuation can be classified by the following five factors.

1. Velocity fluctuation due to the exclusion effect of the surrounding liquid around individual bubbles. This fluctuation originates from the continuity equation as the component of a potential flow, i.e., potential disturbance. It depends on the translational motion of the bubble. The amplitude of the velocity fluctuation is in inversely proportional to the volume fraction of the continuous phase.
2. Velocity fluctuation induced by a wake around an individual bubble. Namely, this fluctuation is caused by a vorticity diffusion from the bubble interface to the downstream of the bubble.
3. Velocity fluctuation produced by unsteady vortex shedding around an individual bubble. This fluctuation is one of the components of factor (2) in the case of high Reynolds number.
4. Velocity fluctuation accompanied by unsteady deformation of individual bubbles (Bhaga and Weber, 1981). This fluctuation is one of components of factor (3) in the case of high Weber numbers. For instance, a spiral motion and a zigzag motion induce this fluctuation.
5. Velocity fluctuation generated by the discrete arrangement of buoyancy as like in dilute bubbly flows. This fluctuation occurs even if there is no relative velocity between bubbles and the surrounding liquid phase. Murai et al. (2000b,c) reported that the wavelength of the velocity fluctuation is associated with the mean bubble–bubble distance.

A number of discussions regarding the factors of (2)–(5) were reported by many researchers using flow visualization techniques and DNS. However, factor (1) is the most essential component because of the large velocity fluctuation amplitude involved. Actually, according to the experiment of Iguchi et al. (1991), 30–40% of the velocity fluctuation generated by the bubbles is caused by the potential disturbance in a bubbly two-phase jet flow. In their experiment, bubble Reynolds number is around 1000. For the case of lower bubble Reynolds number, the potential disturbance is more dominant than the other factors.

3.2. Previous problems of the two-way coupling in the Eulerian–Lagrangian model

The physical quantities of the dispersed phase are defined at individual dispersion positions in the E–L model, while those of the continuous phase are defined by the averaged values for each grid element. When mass, momentum and energy transfers from the continuous phase to the dispersed phase are considered, ordinary Lagrangian interpolation methods are useful to express the physical quantities of the continuous phase around each dispersion. Higher order interpolation is recommended to simulate accurately the continuous-to-dispersed phase transfer. A novel model using the Langevin equation was also proposed by Pozorski and Minier (1998). Employment of a fine grid system inside the regular grid is also a good idea as explained by Yeh (1990). The E–L expression for the finite element method was demonstrated by Serdakowski and Caswell (1988). Zhou and Leschziner (1999) summarized recent interpolation methods for a curvilinear coordinate system.

On the contrary, when the dispersed-to-continuous phase transfer is computed, the following approaches have been adopted as the simplest ways.

(a) The effect of the dispersion presence is only attributed to single grid elements where a center of gravity of the dispersion exists.

(b) When the volume element of the dispersion strides across several grid elements, the effect of the dispersion presence is attributed to all these grid elements by dividing the dispersion volume into the several parts.

Method (a) is applicable when the dispersion volume is sufficiently small compared to the size of a grid element, while method (b) must be used when the dispersion volume is not negligible. Anyhow, both methods (a) and (b) have the common problem that pulsating velocity fluctuation which is not observed in actual bubbly flows is generated during the dispersion migration through grid interfaces, because the physical quantities of the dispersion is expressed discretely at each grid element. This pulsating velocity fluctuation is named 'numerical pseudo-fluctuation' in this paper. The amplitude of the numerical pseudo-fluctuation is estimated to reach 10–100 times of the true dispersion-generated fluctuation. The numerical pseudo-fluctuation not only makes the simulation very unstable but also falsifies the dispersion motion due to the feed-back effect. In order to overcome this problem, it is necessary to adequately construct a numerical coupling method. To this end, Andrews and O'rourke (1996) proposed a new coupling based on the particle-in-cell (PIC) method. They used a linear interpolation function between two grid elements which involves a Lagrangian particle in order to obtain the Eulerian variables of the particle. Their method was examined by testing several cases of one-dimensional flow. The authors (Murai et al., 2000a) tried to remove the numerical pseudo-fluctuation by using the template-distribution (TD, in abbreviation) method in a multi-dimensional space. In the TD method, a template with the same size as that of grid element volume (grid element area in the case of two-dimensional analysis) is utilized to transform the individual physical dispersion quantities to the Eulerian frame. Several neighboring grid elements which overlap with the template receive linear-interpolated components of the physical dispersion quantities. Also since the center of gravity of the template moves with each dispersion migration, numerical diffusion does not happen. Although the authors succeeded in removing the numerical pseudo-fluctuation with the TD method, the amplitude of the velocity fluctuation and the fluctuation waveform were not in good agreement with the true fluctuation. Furthermore, the detailed flow structure which would be evaluated by spatial derivative quantities, such as vorticity and shear strain rate, were not validly predicted by the TD method because the TD method only ensures the first order continuity of the dispersion quantities in space in the same way as the PIC method of one-dimensional tests by Andrews and O'rourke (1996).

3.3. New methods for calculating the local volume fraction

In this section, a new technique which ensures the accurate transfer from a dispersion to carrier phase is explained. Basically, the most important parameter which governs the two-way interaction is the local volume fraction of the dispersed phase, therefore, let us focus on a new definition of the local volume fraction. The velocity and the size of the dispersion can be defined and transformed by using the same principle. Before explaining the new method, we have to state the following two conditions for the new definition.

1. *Conservation*: The total amount of the local volume fraction must not be changed by dispersion migration. This is necessary condition to keep the numerical conservation of mass and momentum.
2. *Continuity*: The spatial distribution of the local volume fraction must have nth order continuity. Here n is the class number of spatial differentiability.

For example, when the volume division methods (a) and (b) described in Section 3.2 are employed, the volume fraction is conserved but it does not ensure the continuity. When a smoothing

filter such as a median or averaging filter is imposed to the results of (a) and (b), the continuity is ensured to some degree but the conservation is not satisfied. On the contrary, when the TD method is applied, the conservation and continuity of first order $(n = 1)$ are satisfied simultaneously. In order to ensure further higher order continuity, the following two kinds of template filtering functions are proposed.

1. Gausssian filtering function [template-distribution method with Gaussian function (TD-G method, in abbreviation)].
2. Sinewave filtering function [template-distribution method with sinewave function (TD-S method, in abbreviation)].

The template filtering function is defined for each center of gravity of the dispersion like as in the previous linear interpolation (i.e., TD) method. Fig. 1 shows a conceptual figure of the two methods. By using the template filtering function, the dispersion volume V which exists at an arbitrary position is divided into surrounding grid elements in each direction x, y, and z. When the dispersion migrates, the surrounding volume fraction changes according to the template filtering function. The local volume fraction, therefore, varies always continuously while the dispersion migrates inside a grid element or passes through a grid interface. By the way, Gaussian function has an infinite profile in space in contrast to sinewave function with a period. So that the position which has less than 0.01 of the peak value of the Gaussian function is ignored. In this case, Gaussian function is slightly amplified to keep exactly the total volume of dispersion in the Eulerian frame. In this point, the sinewave function is numerically suitable as a compact filtering function since it requires only a few grid elements.

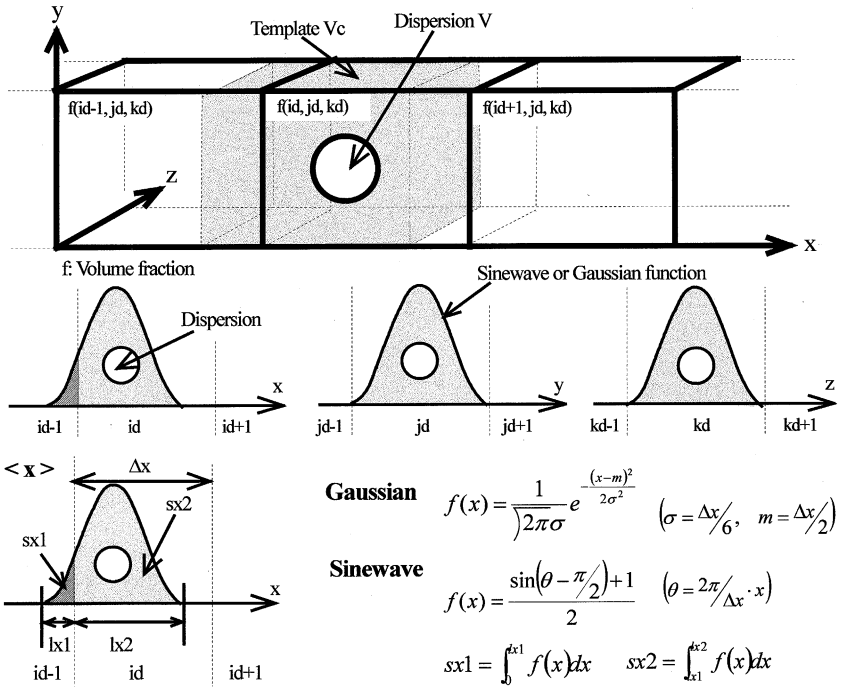

Fig. 1. TD algorithm with Gaussian function and sinewave for the template function.

3.4. Computation of local volume fraction, liquid velocity, and liquid acceleration using new methods

In the E–L model, when the local volume fraction of the dispersion fluctuates, the liquid velocity at the grid interface is computed by Eq. (20) which is a discretized form of the mass conservation equation (19) for incompressible liquids:

$$\frac{\partial(1-\alpha)}{\partial t} + \nabla \cdot (1-\alpha)\mathbf{u}_{\mathrm{L}} = 0, \tag{19}$$

$$u'_{\mathrm{L}} = \frac{\alpha^{n+1} - \alpha^{n}}{\Delta t} \Big/ \left(2(1-\alpha^{n}) \left(\frac{1}{\Delta x} + \frac{1}{\Delta y} + \frac{1}{\Delta z} \right) \right), \tag{20}$$

where $\mathbf{u}_{\mathrm{L}}$ in Eq. (19) is the velocity vector and the subscript L stands for the liquid phase. α is the local volume fraction of dispersion, and Δx, Δy, and Δz are the grid width in each direction.

Fig. 2 shows a time history of the local volume fraction in a control volume obtained by each method. The time is normalized by the time which the dispersion spends to pass a grid. Fig. 3

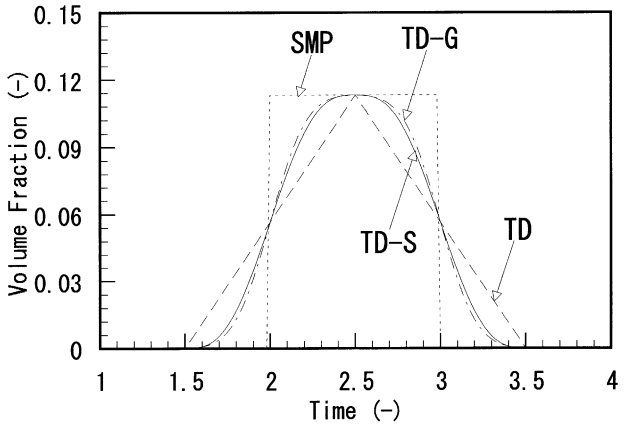

Fig. 2. Local volume fraction in the control volume obtained by each method.

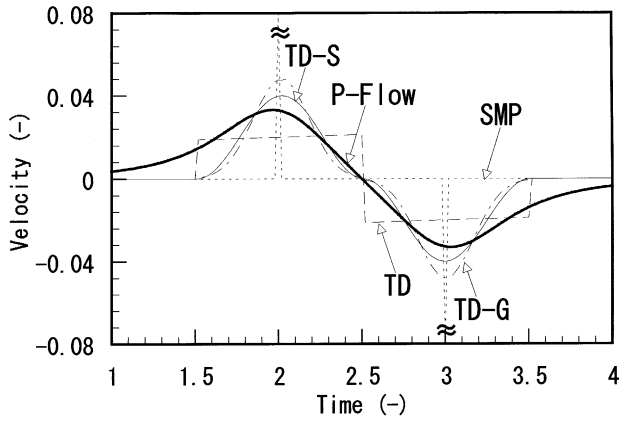

Fig. 3. Liquid velocity exit component $\mathbf{u}'_{\mathrm{L}}$ at the grid interface.

shows the outward liquid velocity component u'_L at the grid interface calculated by Eq. (20). The liquid velocity is normalized by the dispersion's passing velocity. Fig. 4 shows the outward liquid acceleration component normalized by the acceleration given by the dispersion's velocity and the passing time. As a referential value for comparison, the 'P-Flow' in the figures expresses a waveform calculated from the three-dimensional potential flow around a fluid sphere which moves with a constant velocity. The equation of Hill's spherical vortex given by the following equation is used for comparison:

$$\Psi = \frac{1}{2} U_S \left(r^2 - \frac{R^3}{r} \right) \sin^2 \theta, \quad r > R, \tag{21}$$

where U_S is the relative velocity of the dispersion against the continuous phase, r is the distance from the center of gravity of the dispersion, and R is the dispersion radius. Hill's spherical vortex is irrotational outside the sphere, hence, it cannot be the model for a turbulent eddy generated by dispersion. However, it approximates roughly the flow generated by dispersion migration in the case of intermediate Reynolds number without flow separation. At least, it satisfies equation of continuity, the potential disturbance solved by the present two-way coupling method can be examined.

The 'SMP' in Fig. 2 represents the result without the TD method, i.e., the simplest method (1) mentioned in Section 3.2. The 'TD' in Fig. 2 represents the result obtained by the linear TD method, 'TD-G' and 'TD-S' represent the results obtained by the TD method with Gaussian and sinewave filtering functions, respectively. The ratio of the dispersion volume to the grid volume is 0.11 in this case. The results allow the following conclusions:

In the SMP method, the pulsating velocity occurs when dispersion passes through the grid interface. The maximum velocity is around 20 times the peak velocity of the potential flow. In the TD method, though the maximum velocity is decreased, rapid change of the liquid velocity still remains. The results obtained by the TD-G and the TD-S methods have no stepwise waveform.

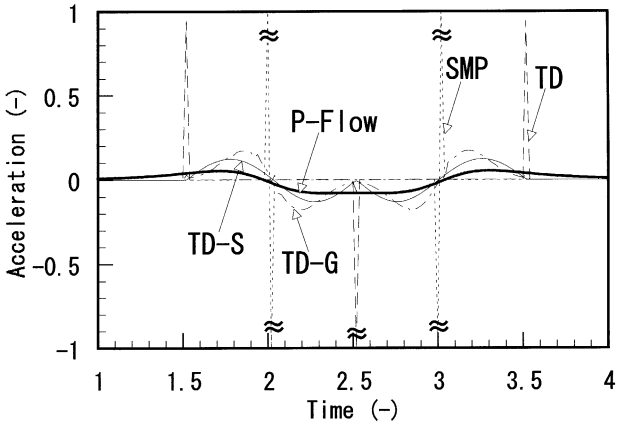

Fig. 4. Exit component of the acceleration of the liquid phase at the grid interface.

By differentiating the velocity waveform with respect to time, the acceleration of the liquid is obtained as shown in Fig. 4. While the SMP method and the TD method produce pulse-like waveforms in the result, the TD-G and the TD-S methods result in reasonable fluctuations. The best method that we can choose through the results of Figs. 3 and 4 is the TD-S method because it provides the best approximated waveforms for the potential flow.

3.5. Relationship between the volume fraction and the maximum velocity of the liquid phase

In order to summarize the aforementioned characteristics, the relationship between the local volume fraction and the maximum absolute velocity of liquid phase is computed as shown in Fig. 5. In this test case, migration of Hill's spherical vortex perpendicular to the grid interface is examined. Computation is performed in three-dimensional space, and the ratio of the dispersion volume V_G to the grid volume V_C, i.e., V_G/V_C is varied to consider the grid dependency. Also r in the figure means the ratio of the dispersion radius to the grid length. The following features emerge.

1. The maximum velocity increases as the (V_G/V_C) ratio increases. This agrees with the solution of the potential flow.
2. The maximum velocity which is obtained by the SMP method is around 20 times as large as the solution of the potential flow for all the treated ranges.
3. The maximum velocity with the TD method is underestimated compared to the potential flow.
4. The TD-S method yields results the most closely related to the potential flow in all the treated ranges. This means that the TD-S method is the best approximation independently on the volume ratio V_G/V_C.

The above results are only confirmed in the case of perpendicular migration of the dispersion relative to the grid interface. According to the additional analysis for oblique passing of dispersion to the grid interface, the maximum velocity has been changed only around 20% from the above-mentioned result. This change is much smaller than difference in choosing the coupling method.

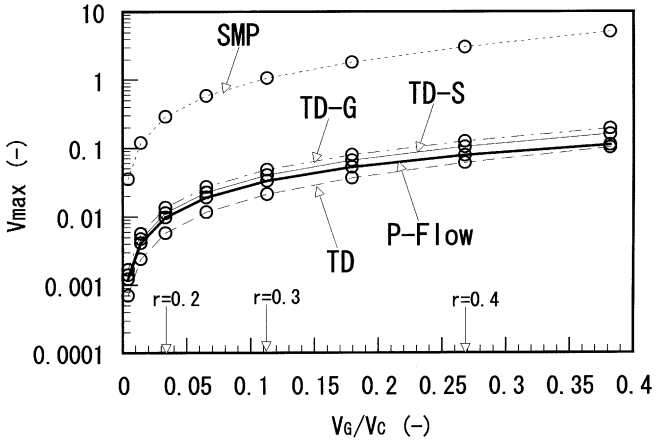

Fig. 5. Relation between local volume fraction and maximum velocity of liquid phase.

Therefore, it can be concluded that the introduction of the higher order filtering function produces much better liquid phase fluctuations than the conventional methods.

3.6. Three-dimensional two-way simulation of a single rising bubble

In this section, we will examine how the two-way coupling method governs the dispersion motion. The objective flow is a single rising bubble motion in a quiescent liquid, which has a constant terminal velocity without unsteady fluctuation. This flow field is quite simple but suitable for strictly evaluating the two-way coupling method. Three kinds of coupling methods, the SMP method, the TD method and the TD-S method, are compared here. Table 1 shows the simulation conditions. Both the initial velocity of the bubble and liquid are 0. Fig. 6 represents the time evolution of the rising velocity obtained by the three methods. The following conclusions can be made.

1. A pulsating fluctuation of around 60% to the average rising bubble velocity is generated during the bubble passing the grid interfaces in the case of the SMP method. This fluctuation is caused by a feed-back effect of the numerical pseudo-fluctuation.

Table 1
Simulation conditions for three-dimensional bubbly flow

Calculation domain	$0.1\ \text{m} \times 0.1\ \text{m} \times 0.1\ \text{m}$
Grid division number	$48 \times 48 \times 48$
Time integration step	0.0005 s
Simulation period	2.0000 s
Kinematic viscosity of the liquid	$10^{-6}\ \text{m}^2/\text{s}$
Gravitational acceleration	$9.806\ \text{m}/\text{s}^2$
Gas density	$0\ \text{kg}/\text{m}^3$
Liquid density	$10^3\ \text{kg}/\text{m}^3$
Bubble radius	0.3 mm

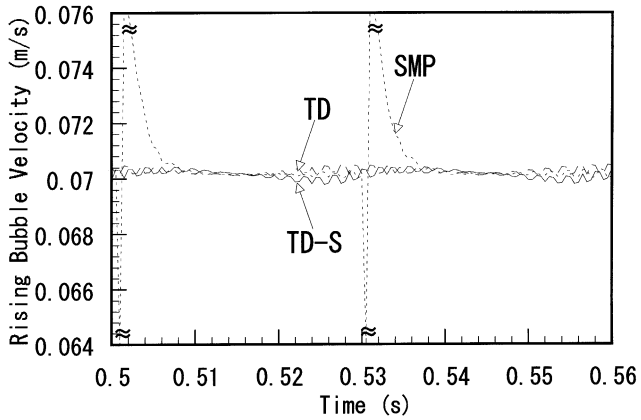

Fig. 6. Time evolution of rising bubble velocity obtained by each method.

Table 2
Comparison of results obtained by each method

	Local volume fraction		Continuity of liquid	$\lvert V_G - \overline{V}_G \rvert_{max}/\overline{V}_G$ (%)
	Continuity	Conservation		
SMP	×	○	×	62.8
TD	○	○	×	0.4
TD-S	○ (higher order)	○	○	0.5

○: satisfactory; ×: unsatisfactory.

2. Although a slight velocity fluctuation is still observed in the cases of the TD and TD-S methods, the amplitude is much reduced in comparison with the SMP method. The small fluctuation depends on the differentiation scheme of the translational bubble motion. For example, the lower order differentiation derives a low-accuracy result but a smoothed waveform while the higher order differentiation derives higher accuracy but a partially oscillatory waveform. Anyway, the slight error is not serious compared to the effective improvement due to the filtering functions.

Table 2 summarizes the characteristics of the three coupling methods. The upper right column in the table is the ratio of rms fluctuation velocity to the average velocity. It is concluded that the TD-S method ensures both continuity and conservation of the local volume fraction, and also the false velocity fluctuations of continuous and dispersed phases are satisfactorily removed.

4. Applications to bubbly flow, particulate flow, and three-phase flow

In this section, the proposed method is applied to the two-way simulation of a dispersion-generated fluctuation. The objective flow in this section is natural convection induced by the body forces of many bubbles and solid particles. No main liquid flow or a solid wall boundary is introduced. Therefore, only the structure of the dispersion-generated fluctuation is focused on. The simulation conditions are summarized in Table 3. α_T, α_G, and α_S in the table are the total volume fractions of the three-phase flow, bubbly flow and particulate flow, respectively. N_G and N_S are the total numbers of the bubbles and the particles, respectively. The initial condition is as follows: the liquid is quiescent, all the dispersions are randomly located, and the velocity of the dispersion is 0. All the six boundaries of the computational domain are completely periodic both for the continuous and the dispersed phases. The maximum Reynolds number of the dispersion is around 100.

Before describing the analysis, experimental photographs of the dispersion-generated fluctuation are shown in Figs. 7(a) and (b). Detailed experimental conditions are described in the figure-caption. The pathlines of tracer particles are visualized by a sheet of light whose thickness is 5 mm. The tracer particles are made of spherical high porous polymer with 1010 kg/m^3 in density and 250–400 μm in diameter. They indicate the presence of vortical structures in the interval space of the dispersions for the both cases (a) and (b). The typical length of the vortex is much longer than the dispersion size and corresponds roughly with the dispersion distance. Therefore, it is confirmed from this observation that the assumptions for the E–L model are valid for the application.

Table 3
Simulation conditions for three-dimensional analysis

Calculation domain	$0.1\ \mathrm{m} \times 0.1\ \mathrm{m} \times 0.1\ \mathrm{m}$	
Grid division number	$48 \times 48 \times 48$	
Time integration step	0.0005 s	
Simulation period	4.0000 s	
Kinematic viscosity of liquid	$10^{-6}\ \mathrm{m}^2/\mathrm{s}$	
Gravitational acceleration	$9.806\ \mathrm{m}/\mathrm{s}^2$	
Gas density	$0\ \mathrm{kg}/\mathrm{m}^3$	
Liquid density	$10^3\ \mathrm{kg}/\mathrm{m}^3$	
Solid density	$2 \times 10^3\ \mathrm{kg}/\mathrm{m}^3$	
For bubbly flow		$\alpha_G \fallingdotseq 2.6180\%$ ($N_G = 50,000;\ R = 0.5$ mm)
For particulate flow		$\alpha_S \fallingdotseq 2.6180\%$ ($N_S = 50,000;\ R = 0.5$ mm)
For three-phase flow	Case 1	$\alpha_T \fallingdotseq 0.0042\%$ ($N_G = 5000,\ N_S = 5000;\ R = 0.1$ mm)
	Case 2	$\alpha_T \fallingdotseq 0.3393\%$ ($N_G = 15,000,\ N_S = 15,000;\ R = 0.3$ mm)
	Case 3	$\alpha_T \fallingdotseq 2.6180\%$ ($N_G = 25,000,\ N_S = 25,000;\ R = 0.5$ mm)

R: dispersion radius.

4.1. Structure of the two-way dispersion-generated velocity fluctuation

Fig. 8 shows the iso-surface structure of enstrophy in the liquid phase for the three cases of three-phase flow. In this simulation, the possibility of collision between bubbles and particles in the case (c) is not low in the actual situation because of counter-current motion. However, the effect of collision is ignored here by two reasons. That is, (1) general statistic or deterministic model of bubble–particle collision is not established yet. The collision pattern is governed by micro-scale flow in a liquid film between two surfaces of dispersions as well as electric and chemical properties of the surfaces. (2) The collision pattern is not so elastic due to the liquid film

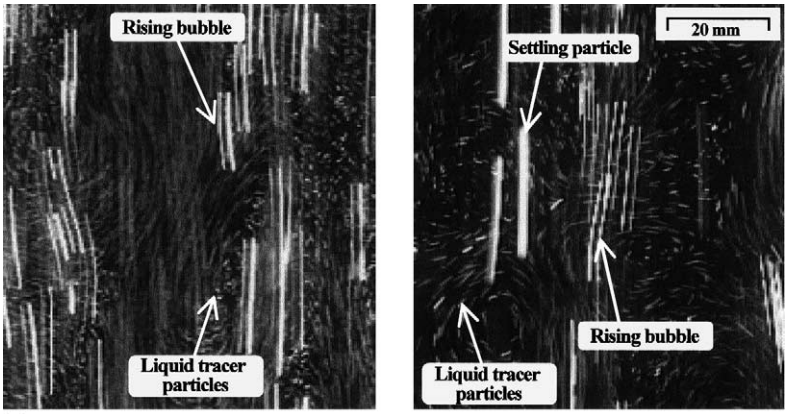

Fig. 7. Experimental image of liquid fluctuation: (a) bubbly flow; (b) three-phase flow. Experimental conditions of bubbly flow are $\alpha_G = 0.612\%$, $R_G = 0.64$ mm, and $R'_G = 0.15$ mm, while those of three-phase flow are $\alpha_T = 0.529\%$, $R_G = 0.82$ mm, $R_S = 0.98$ mm, $R'_G = 0.21$ mm, and $R'_S = 0.02$ mm.

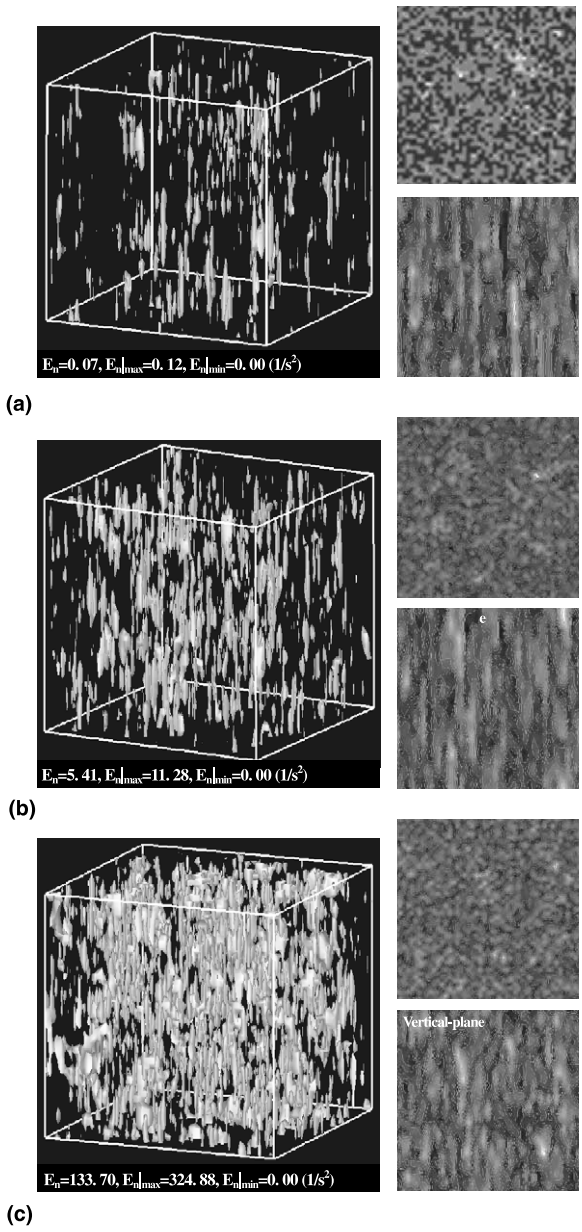

Fig. 8. Iso-surface structure of enstrophy in liquid phase induced by bubbles and particles: (a) case 1 [$\alpha_T \fallingdotseq 0.0042\%$ ($N_G = 5000$, $N_S = 5000$; $R = 0.1$ mm)]; (b) case 2 [$\alpha_T \fallingdotseq 0.3393\%$ ($N_G = 15,000$, $N_S = 15,000$; $R = 0.3$ mm)]; (c) case 3 [$\alpha_T \fallingdotseq 2.618\%$ ($N_G = 25,000$, $N_S = 25,000$; $R = 0.5$ mm)]. Enstrophy E_n is defined as $|\nabla \times \mathbf{u}_L|^2/2$.

that the displacements of collided dispersions are sufficiently short in comparison with grid size. Hence, the grid-averaged quantities such as mass and momentum are not greatly affected even if the collision model is introduced.

As the dispersion volume fraction becomes larger, (a)–(c) of the figure, the enstrophy is rapidly increased to higher values and the flow structure becomes like a turbulent flow involving small eddies. This complicated flow is one of typical structures of so-called pseudo-turbulence. In this case, the pseudo-turbulence has long wave length in the vertical direction because of rising bubbles and settling particles. Right parts in the figure represent instantaneous enstrophy distribution in the horizontal and vertical cross-sections. The enstrophy is isotropic in the horizontal plane while it is heterogeneous in the vertical cross-section. It means that the horizontal velocity fluctuation is caused by the potential disturbance as mentioned in Section 3, while vertical velocity fluctuation is induced by combination of the potential disturbance and body force.

Fig. 9 shows bubbles (○), particles (●) and enstrophy distributions in a vertical cross-section. In this figure, three kinds of dispersed flow are shown: (a) for bubbly two-phase flow, (b) for particulate two-phase flow, and (c) for bubble–particle three-phase flow. The total volume fraction of dispersion is all 2.618%, and the radius of the dispersion is 0.5 mm for all the three cases (see Table 3 for detailed condition). The figures are drawn after the flow field becomes sufficiently developed (at $t = 4.0$ s). The judgment of the flow's development is done by monitoring the wave spectrum of the liquid velocity field. The following points can be confirmed.

1. The bubble distribution in the case of bubbly flow (see Fig. 9(a)) seems to be forming bubble clusters. Although no bubble–bubble interaction model is directly introduced in the present E–L model, the bubble clusters can be generated by the local pressure gradient in the region which has a high enstrophy. The pressure gradient force acting on the bubble due to the enstrophy is much weaker than that due to gravity, so that it takes a few seconds to observe the bubble clusters.
2. In the particulate flow, the local maximum of enstrophy is larger than that of the bubbly flow (see gray level in Fig. 9(b)). This difference is related to the status of the particle distribution. That is, the particles will be scattered more uniformly than the bubbles since inertia force is larger than that of the surrounding fluid. Therefore, the particles accumulate rather in the high strain rate region than high enstrophy region (e.g., Squires and Eaton, 1990; Wang and Maxey, 1993). Also they allow us to keep up the high enstrophy structure while the bubbles do not produce the high enstrophy region because body force of the particle acts outside of each rotational motion of the liquid. The lift force of the particle which is stronger than that of the bubbles is also the factor to enhance the scattered distribution.
3. In the case of bubble–particle three-phase flow (see Fig. 9(c)), the maximum of enstrophy is weaker than that of the particulate flow. The order of the magnitude is as same as bubbly two-phase flow. However, the bubbles in the three-phase flow do not cause bubble clusters clearly. The reason is that the flow structure of liquid phase is significantly altered by momentum interaction with particles. This is said just a two-way interaction phenomenon which is not to be predicted by one-way analysis or linear overlapping of two kinds of flow structure, i.e., bubbly and particulate two-phase flows.

Fig. 10 shows the probability density profiles of dispersion in three-phase flow regarding to the enstrophy of liquid phase at $t = 4.0$ s. The probability Γ is normalized by that of liquid phase, hence, $\Gamma > 1$ means that the dispersion concentrates in the corresponding enstrophy region, and $\Gamma < 1$ means that it avoids the region. It is confirmed from the result that the bubbles distribute in

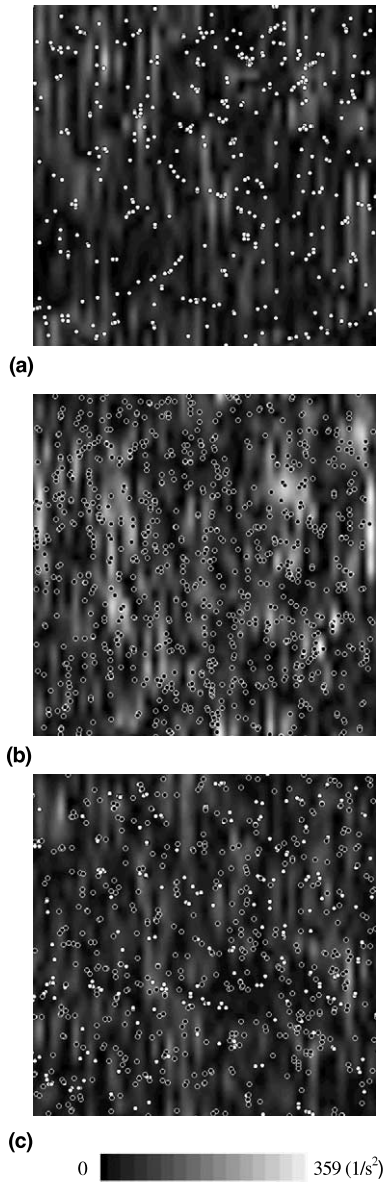

Fig. 9. Enstrophy distribution in liquid phase and dispersion in a vertical cross-section: (a) bubbly flow [$\alpha_G \fallingdotseq 2.618\%$ ($N_G = 50,000,\ R = 0.5$ mm)]; (b) particulate flow [$\alpha_S \fallingdotseq 2.618\%$ ($N_S = 50,000,\ R = 0.5$ mm)]; (c) three-phase flow [$\alpha_T \fallingdotseq 2.618\%$ ($N_G = 25,000,\ N_S = 25,000,\ R = 0.5$ mm)] (○, bubble; •, particle; gray-scale, enstrophy, i.e., $|\nabla \times \mathbf{u}_L|^2/2$).

high enstrophy region while the particles do not there. Since these characteristics were reported by many researchers using DNS (e.g., Squires and Eaton, 1990; Wang and Maxey, 1993; Druzhinin and Elghobashi, 1998), it is concluded that the present method has high applicability for simulating detailed flow structure.

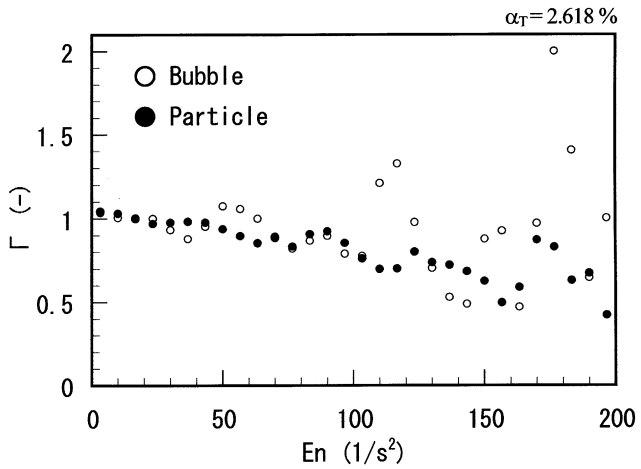

Fig. 10. Probability density profiles of dispersion in three-phase flow regarding to the enstrophy of liquid phase at $t = 4.0$ s. E_n is enstrophy defined as $|\nabla \times \mathbf{u}_L|^2/2$. Γ is probability of dispersion's presence at arbitrary enstrophy of liquid phase, normalized by that of liquid phase.

4.2. Rising and settling velocity of dispersions in the dispersion-generated velocity fluctuation

Fig. 11 shows a time evolution of the absolute value of average rising bubble velocity and the average settling particle velocity in each entire flow field. The notes of 'Bubble(B-Flow)', 'Particle(P-Flow)', 'Bubble(T-Flow)', and 'Particle(T-Flow)' in the figure represent the bubble's velocity in the bubbly flow, the particle's velocity in the particulate flow, and the bubble's and the particle's velocities in the three-phase flow, respectively. Although the sizes of the bubble and the particle are the same, their terminal velocities in quiescent liquid are different due to the different drag coefficient.

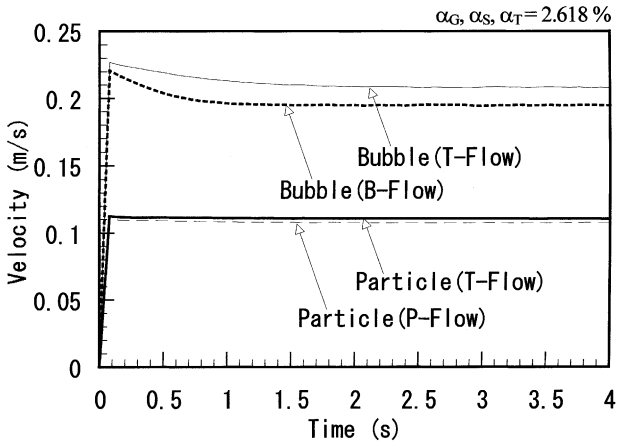

Fig. 11. Time evolution of the average rising bubble velocity and the average settling particle velocity in each flow field.

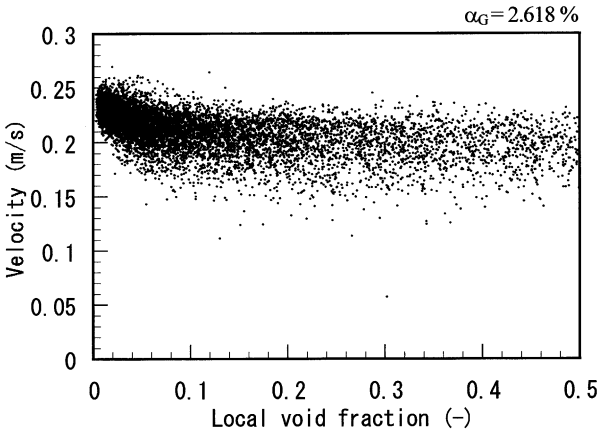

Fig. 12. Relation between the bubble rising velocity and the local gas volume fraction in bubbly flow.

In the transitional stage after starting the simulation, both bubble and particle motions are rapidly accelerated. Then the bubble velocity is slowly reduced by the effect of the two-way interaction while the particle velocity is kept almost constant. In the quasi-steady state after $t = 2$ s, the rising velocity of a bubble in the three-phase flow is faster than that of a bubble in the bubbly flow. This difference occurs due to whether bubbles generate bubble clusters or not as mentioned in the previous section. For the evidence, the relationship between the bubble rising velocity and the local gas volume fraction in bubbly flow is shown in Fig. 12. The bubble rising velocity decreases as local volume fraction of bubble increases. The decrease of the bubble velocity is explained by the reduction of the local pressure gradient (i.e., the gravity term in Eq. (6)) in the clustering case. The average particle velocity in the three-phase flow is almost unchanged compared to that of particulate flow because the particles are uniformly distributed.

4.3. Kinetic energy induced by body forces of bubbles and particles

Fig. 13 shows the time evolution of the kinetic energy in liquid phase for the three cases. The kinetic energy is calculated by squared absolute velocity of liquid considering the decrease of liquid volume fraction in the dispersion mixture. This figure confirms that particulate flow has the largest kinetic energy among the three cases. This reason is simply the difference of averaged dispersion velocity as shown in Fig. 11. Namely, the drag of a particle is larger than that of a bubble, so that the dispersion-to-liquid interaction is enhanced. In addition, the scattered particle distribution may also induce effectively velocity fluctuation for a wider region. The kinetic energy of the three-phase flow is almost the same as that of the bubbly flow. This is because the local averaged body force which acts on the liquid flow in the vertical direction is reduced by simultaneous presence of bubbles and particles. This reason corresponds with the spectra of the body force as follows. Figs. 14(a) and (b) show the spectra of the grid-averaged body force for initial condition (a) and for the quasi-steady state at $t = 4.0$ s (b). These spectra are obtained by a Fourier transformation of the body force distribution (gravity term in Eq. (6)) in the entire physical space. The maximum wave number is determined by the inverse number of grid size

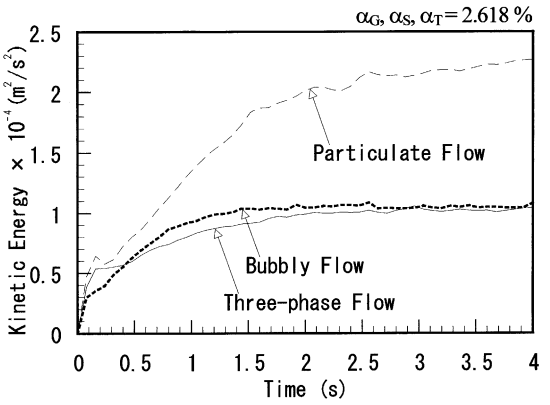

Fig. 13. Kinetic energy of liquid phase for each flow field.

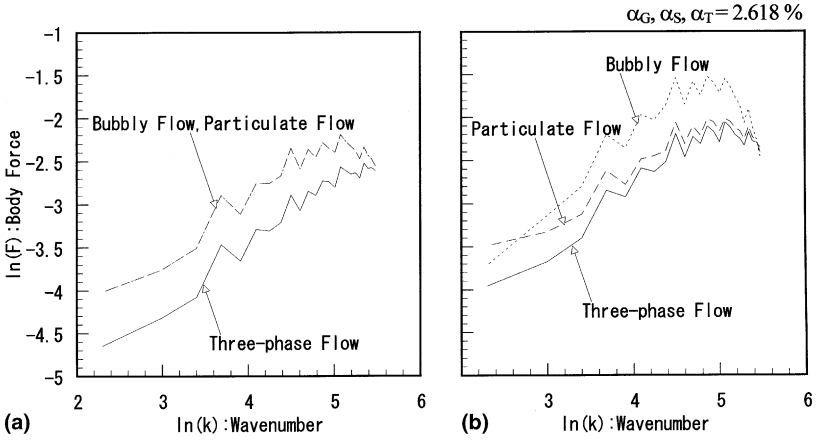

Fig. 14. Body force for bubbly flow, particulate flow and three-phase flow: (a) $t = 0.0$ s; (b) $t = 4.0$ s.

which is larger than dispersion size. Hence, the spectra shown in this figure is that for the wavelength longer than the grid size. In the initial condition in which all the bubbles and the particles are randomly distributed, spectrum of three-phase flow is smaller in comparison to that of the other two-phase flow. This is owing to the offset effect between the buoyancy of the bubbles and the weight of the particle. In the quasi-steady state (b), the bubbly flow has a higher spectrum in the high wave number region than the other types of flow. This is due to the bubble clustering effect which induces wavy fluctuation of body force. The wave number of the spatial fluctuation is determined by that of the cluster size and it ranges from $k = 50$ to 150 m^{-1}, i.e., $\ln(k) = 4$ to 5. Thus, the bubbly flow would generate higher velocity fluctuation than the others if the drag and the lift forces on the bubble were set the same as those on the particle.

By the way, the data of these spectra can be validly obtained by using the present TD-S method. When the simple definition of the dispersion volume fraction was daringly used, the spectra had abnormally high value in the high wave number region, and its numerical simulation was

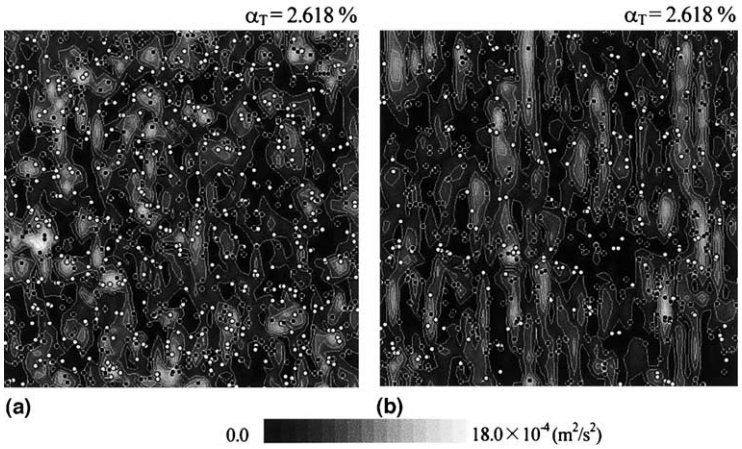

Fig. 15. Kinetic energy distribution in liquid phase and dispersions in a vertical cross-section: (a) SMP; (b) TD-S.

sometimes broken down in the midway before reaching quasi-steady state. Fig. 15 is the comparison of three-phase flow structure between simple definition, SMP (a) and TD-S method (b). Kinetic energy of liquid is too large in the swarm of dispersions in the case of simple definition. This is also recognized by the time evolution of the kinetic energy as shown in Fig. 16. The kinetic energy must increase continuously but that obtained by simple definition suddenly increases in initial transient stage and keeps too high value after 0.1 s.

Finally, the grid dependency of the present model is examined using two kinds of grid division numbers, 36^3 and 48^3. The result is summarized in Table 4 and each value is time-averaged for 1.0 s from 3.0 s. As the principle of grid-averaged model, the amplitude of dispersion-generated fluctuation velocity of liquid phase depends on the volume ratio of the dispersion to grid as explained in 3.5. However, the resultant data have good agreement between the two results. This means, the numerical stability and accuracy are significantly improved by introducing the filtering

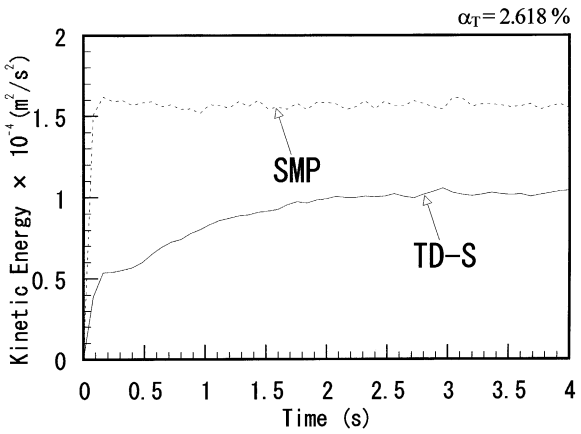

Fig. 16. Kinetic energy of liquid phase in three-phase flow for each method.

Table 4
Examination of grid dependency

Grid division number	K_G (m^2/s^2)	K_S (m^2/s^2)	K_T (m^2/s^2)	$\lvert V_{B\text{-}B}\rvert$ (m/s)	$\lvert V_{P\text{-}P}\rvert$ (m/s)	$\lvert V_{T\text{-}B}\rvert$ (m/s)	$\lvert V_{T\text{-}P}\rvert$ (m/s)
$36 \times 36 \times 36$	1.065×10^{-4}	2.738×10^{-4}	1.195×10^{-4}	0.203	0.110	0.219	0.113
$48 \times 48 \times 48$	1.050×10^{-4}	2.210×10^{-4}	1.022×10^{-4}	0.195	0.108	0.208	0.111

K_G, K_S, and K_T stand for kinetic energy of liquid phase in bubbly flow, particulate flow, and three-phase flow, respectively. $|V_{B\text{-}B}|$ and $|V_{P\text{-}P}|$ stand for absolute averaged rising velocity of bubbles in bubbly flow and absolute averaged settling velocity of particles in particulate flow, respectively. $|V_{T\text{-}B}|$ and $|V_{T\text{-}P}|$ stand for absolute averaged rising velocity of bubbles and absolute averaged settling velocity of particles in three-phase flow.

functions, and simulated flow structure is not sensitively altered by changing the grid division number.

5. Conclusions

In this study, several problems of computing dispersed multiphase flow using the Eulerian–Lagrangian (E–L) model were explained and a new two-way coupling method was proposed. As an application, structures of dispersion-generated velocity fluctuation were demonstrated. Through the present investigation, the following points have been clarified.

1. When a Lagrangian filtering function is used to calculate the spatial volume fraction of dispersion, the velocity fluctuation of the continuous phase due to the individual dispersion migration through Eulerian frames can be accurately obtained. The filtering functions based on a Gaussian distribution (TD-G) and a sinewave distribution (TD-S) ensure much better waveforms of the velocity fluctuations than conventional simple methods. After the appropriate solution for the velocity fluctuation of the continuous phase can be obtained, the false velocity fluctuation of the dispersion is also removed.
2. The filtering function using the sinewave is recognized as the best method because of two reasons: (a) the maximum velocity fluctuation agrees best with a potential flow (i.e., potential disturbance) for a wide range of sphere sizes; (b) the sinewave function is easily introduced to converting the volume fraction of dispersion because it is a compact filtering function using a few grid elements.
3. Detailed flow structure of dispersion-generated velocity fluctuation can be predicted by using the present new E–L model. There is no erroneous behavior found in the results when total volume fraction is under 3.0%. Several features of three kinds of dispersed multiphase flow are demonstrated. As described in Section 4, some discussion could be made on the relationship among the flow fluctuation of continuous phase, dispersion's motion, and spectrum of body force.

Acknowledgements

This work is supported through the Grant-in-Aid for Scientific Research (C.No. 10650166) by the Ministry of Education, Science and Culture, Japan.

References

Andrews, M.J., O'rourke, P.J., 1996. The multiphase particle-in-cell (MP-PIC) method for dense particulate flows. Int. J. Multiphase Flow 22, 379–402.

Auton, T.R., 1987. The lift force on a spherical body in a rotational flow. J. Fluid Mech. 183, 199–218.

Batchelor, G.K., 1967. An Introduction to Fluid Dynamics. Cambridge University Press, Cambridge.

Bhaga, D., Weber, M.E., 1981. Bubbles in viscous liquid: shapes, wakes and velocities. J. Fluid Mech. 105, 61–85.

Brauer, H., Mewes, D., 1972. Strömungswiderstand sowie stationärer und instationärer Stoff- und Wärmeübergang an Kugeln. Chem. Ing. Tech. 44, 865–868.

Decker, S., Sommerfeld, M., 2000. Numerical calculations of two-phase flows in agitated vessels using the Euler/Lagrange approach. In: Proc. ASME 2000 Fluids Engineering Division Summer Meeting, No. FEDSM2000-11154/CD-ROM, pp. 1–8.

Druzhinin, O.A., Elghobashi, S., 1998. Direct numerical simulation of bubble-laden turbulence flows using the two-fluid formulation. Phys. Fluids 10 (3), 685–697.

Elghobashi, S., Truesdell, G.C., 1993. On the two-way interaction between homogeneous turbulence and dispersed solid particles. I. Turbulence modification. Phys. Fluids A 5, 1790–1801.

Iguchi, M., Takeuchi, H., Morita, Z., 1991. The flow field in air–water vertical bubbling jets in a cylindrical vessel. ISIJ Int. J. 31, 246–253.

Kunugi, T., 1997. Direct numerical algorithm for multiphase flow with free surfaces and interfaces. In: Proc. ISAC'97, JSME Centenial Grand Congress, 25–30.

Moissette, S., Oesterle, B., Boulet, P., 2000. Simulation of particle temperature fluctuations in Eulerian–Lagrangian predictions of heat transfer in a turbulent gas–solid pipe flow. In: Proc. ASME 2000 Fluids Engineering Division Summer Meeting, No. 11143/CD-ROM, pp. 1–8.

Murai, Y., Matsumoto, Y., Song, X-Q., Yamamoto, F., 2000a. Numerical analysis of turbulence structures induced by bubble buoyancy. JSME Int. J. Ser. B 43 (2), 180–187.

Murai, Y., Kitagawa, A., Song, X-Q., Yamamoto, F., Ohta, J., 2000b. Inverse energy cascade structure of turbulence in a bubbly flow (numerical analysis using Eulerian–Lagrangian model equations). JSME Int. J. Ser. B 43 (2), 197–205.

Murai, Y., Song, X-Q., Takagi, T., Ishikawa, M., Yamamoto, F., Ohta, J., 2000c. Inverse energy cascade structure of turbulence in a bubbly flow PIV measurement and results. JSME Int. J. Ser. B 43 (2), 188–196.

Nadaoka, K., Nihei, Y., Yagi, H., 1999. Grid-averaged Lagrangian LES model for multiphase turbulent flow. Int. J. Multiphase Flow 25, 1619–1643.

Pan, Y., Banerjee, S., 1997. Numerical investigation of the effects of large particles on wall-turbulence. Phys. Fluids 9, 3786–3807.

Pozorski, J., Minier, J.-P., 1998. On the Lagrangian turbulent dispersion models based on the Langevin equation. Int. J. Multiphase Flow 24, 913–945.

Ransom, V.H., 1985. RELAP/MOD2 Code Manual. Vol. 1. Code Structure, System Models, and Solution Methods. NUREG/CR-4312, EGG-2796.

Reutsch, G.R., Meiburg, E., 1994. Two-way coupling in shear layers with dilute bubble concentration. Phys. Fluids A 6, 2656–2670.

Saffman, P.G., 1965. The lift on a small sphere in a slow shear flow. J. Fluid Mech. 22, 385–400.

Serdakowski, J.A., Caswell, B., 1988. Finite element Eulerian–Lagrangian method for time dependent flow of multimode fluids. J. Non-Newtonian Fluid Mech. 29, 217–244.

Squires, K.D., Eaton, J.K., 1990. Particle response and turbulence modification in isotropic turbulence. Phys. Fluids A 2 (7), 1191–1203.

Sugiyama, K., Matsumoto, Y., 1998. Large eddy simulation of bubbly turbulent channel flow. In: Proc. 3rd Int. Conf. on Multiphase Flow (ICMF'98-Lyon), Paper No. 280/CD-ROM, pp. 1–7.

Sussman, M., Smerka, P., Osher, S., 1994. A level set approach for computing solutions to incompressible two-phase flow. J. Comp. Phys. 114 (1), 146–159.

Takagi, S., Matsumoto, Y., 1996. Force acting on a spherical bubble rising through a quiescent liquid. J. Multiphase Flow 10 (3), 264–273 (in Japanese).

Takemura, F., Yabe, A., 1997. Terminal velocity of spherical gas bubbles below Reynolds number of 100. Trans. Jpn. Soc. Mech. Eng. 63, 2909–2914 (in Japanese).

Takewaki, H., Yabe, T., 1987. The cubic-interpolated pseudo particle (CIP) method: application to nonlinear and multi-dimensional hyperbolic equations. J. Comp. Phys. 70, 355–362.

Tomiyama, A., Takagi, S., Matsumoto,Y., 1999. Numerical Simulations of Bubble Flows Using Interface Tracking and Bubble Tracking Methods Moving Boundaries V. WIT Press, pp. 191–206.

Tomiyama, A., Zun, I., Sou, A., Sakaguchi, T., 1993. Numerical analysis of bubble motion with the VOF method. Nucl. Eng. Des. 141, 69–82.

Unverdi, S.O., Tryggvason, G., 1992. A front-tracking method for viscous incompressible multi-fluid flows. J. Comput. Phys. 100,, 25–37.

Valentine, J.R., Decker, R.A., 1995. A Lagrangian–Eulerian scheme for flow around an airfoil in rain. Int. J. Multiphase Flow 21,, 639–648.

Wang, L., Maxey, M.R., 1993. Settling velocity and concentration distribution of heavy particles in homogeneous isotropic turbulence. J. Fluid Mech. 256, 27–68.

Yeh, G.T., 1990. A Lagrangian–Eulerian method with zoomable hidden fine-mesh approach to solving advection–dispersion equations. Water Resources Res. 26, 1133–1144.

Zhang, D.Z., Prosperetti, A., 1994. Ensemble phase-averaged equations for bubbly flows. Phys. Fluids 6 (9), 2956–2967.

Zhou, Q., Leschziner, M.A., 1999. An improved particle-locating algorithm for Eulerian–Lagrangian computations of two-phase flows in general coordinates. Int. J. Multiphase Flow 25, 813–825.